ATLAS NOTE

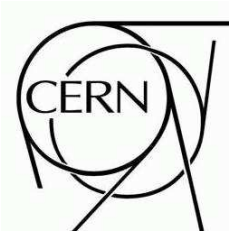

April 28, 2009

Discovery Potential of $h/A/H \to \tau^+\tau^- \to \ell^+\ell^- 4\nu$

The ATLAS Collaboration[1)]

This note is part of CERN-OPEN-2008-020. This version of the note should not be cited: all citations should be to CERN-OPEN-2008-020.

ATL-PHYS-PUB-2009-059
10 May 2009

Abstract

This note describes a study of the discovery potential for the supersymmetric Higgs bosons $h/H/A$ in proton-proton collisions at a center-of-mass energy of 14 TeV in final states with τ lepton pairs with the ATLAS detector at the LHC. The Higgs bosons are produced in association with b quarks and decay into a $\tau\tau$ final state where both τ leptons decay leptonically. The signature of Higgs bosons with masses between 110 and 450 GeV is analyzed and the discovery potential is assessed. The analysis is based on an integrated luminosity of $30\,\text{fb}^{-1}$.

All results are obtained using full simulation of the ATLAS detector. No pile-up or cavern background has been considered in this analysis. In addition a procedure for estimating the shape and the normalization of the irreducible $Z \to \tau^+\tau^-$ background from data is investigated. The discovery potential as a function of m_A and $\tan\beta$ is shown for the m_h^{max} MSSM benchmark scenario.

[1)]This note prepared by: E. Barberio, M. Bischofberger, D. Cavalli, S. Gentile, D.M. Gingrich, E. Gross, M. Kobel, E. Kuznetsova, J. Lu, W.F. Mader, S. Resconi, A.F. Saavedra, J. Schaarschmidt, O.S. Silbert, C. Tamarindi, T. Vickey, M. Warsinsky.

1 Introduction

In the Minimal Supersymmetric Standard Model (MSSM), the minimal extension of the Standard Model, two Higgs doublets are required, resulting in five observable Higgs bosons. Three of them are electrically neutral (h^0 , H^0 , and A^0) while two of them are charged ($H^{\pm}$). At tree level their properties like masses, widths and branching fractions can be predicted in terms of only two parameters, typically chosen to be the mass of the CP-odd Higgs boson, m_A, and the tangent of the ratio of the vacuum expectation values of the two Higgs doublets, $\tan\beta$.

In the MSSM the couplings of the Higgs bosons to fermions and bosons are different from those in the Standard Model resulting in different production cross-sections and decay rates. While decays into ZZ or WW are dominant in the Standard Model for Higgs boson masses above $m_H \sim 160$ GeV, in the MSSM these decay modes are either suppressed like $\cos(\beta-\alpha)$ in the case of the H^0 (where α is the mixing angle of the two CP-even Higgs bosons) or even absent in case of the A^0. Instead, the coupling of the Higgs bosons to third generation fermions is strongly enhanced for large regions of the parameter space. The decay of the neutral Higgs bosons into a pair of τ leptons therefore constitutes an important discovery channel at the LHC. The production of the Higgs bosons can proceed via two different processes: gluon-fusion or production in association with b quarks.

In this note, the discovery potential of neutral MSSM Higgs bosons, produced via associated production with b quarks and decaying into a pair of τ leptons in ATLAS at the LHC is discussed. Only τ lepton decays into electrons and muons are considered here. Higgs bosons in the mass range between 110 and 450 GeV are analyzed for an integrated luminosity of $30\,\text{fb}^{-1}$. Both the shape and the normalization of the $Z \to \tau\tau$ background which is dominant for low Higgs boson masses are estimated from $Z \to \mu\mu$ and $Z \to ee$ events in data. The results are interpreted in the m_h^{max} scenario as a function of the two parameter of the model, m_A and $\tan\beta$ [1]. Studies concerning the semileptonic and the fully hadronic final state are not included in this note. These studies are ongoing and will be published separately.

This note is organized as follows. In Section 2 the signal and background processes are introduced and their cross-sections are discussed. In Section 3 the analysis is discussed. After a description of the selection, a procedure to estimate the shape and the normalization of the irreducible $Z \to \tau^+\tau^-$ background from data is detailed before the discovery potential in the $m_A - \tan\beta$ plane is assessed. In Section 4 the results are summarized.

2 Signal and background processes

2.1 Higgs boson production

The production mechanism of Higgs bosons in the MSSM is discussed in the introductory section of this chapter. The Higgs boson masses, their production cross-section and their branching fraction into a pair of τ leptons are summarized in Table 1.

The theoretical uncertainty on the inclusive production cross-section, i.e. without imposing any requirements on the p_T of the b jets at generator level, is estimated taking into account contributions from the scale uncertainty and from the uncertainty on the parton distribution functions. The scale uncertainty is obtained from Ref. [2] as a function of the mass of the Higgs boson. The contribution from the Parton Density Functions (PDFs) is estimated by exchanging MRST2002 for MRST2004 parton distribution functions. Since the cross-sections obtained with MRST2004 are smaller than that with MRST2002 they are considered conservative. Therefore, half of the difference observed with this variation is taken as a systematic uncertainty.

The total uncertainty on the cross-section, obtained by adding the PDF and scale uncertainties in quadrature, is displayed in Fig. 1 as a function of the Higgs boson mass m_A. For Higgs boson masses as

Table 1: Masses, cross-sections for b-associated production, and branching fractions into the $\tau^+\tau^-$ final state for Higgs bosons in the $m_h^{\max}$ scenario and for $\tan\beta = 20$.

Mass / GeV			$\sigma^{\text{associated}}_{h/H/A}$/fb			$\mathscr{B}(h/H/A \to \tau^+\tau^-)$/%		
A	H	h	A	H	h	A	H	h
110	129.8	109.0	314810	7579	310707	8.9	9.1	8.9
130	134.2	124.7	189602	92897	99992	9.1	9.2	9.0
160	160.8	128.0	97480	93102	6650	9.4	9.5	8.4
200	200.5	128.4	45685	45095	2188	9.6	9.7	7.5
300	300.4	128.6	10312	10253	979	8.2	9.5	6.3
450	449.8	128.6	2019	2035	723	6.1	6.2	5.7

low as $m_A = 100$ GeV the total theoretical uncertainty is of the order of 20%. This uncertainty decreases to values below 10% for $m_A = 400$ GeV. For low Higgs boson masses the contribution from the scale uncertainty dominates over that from the parton distribution functions while for high Higgs boson masses the situation is reversed.

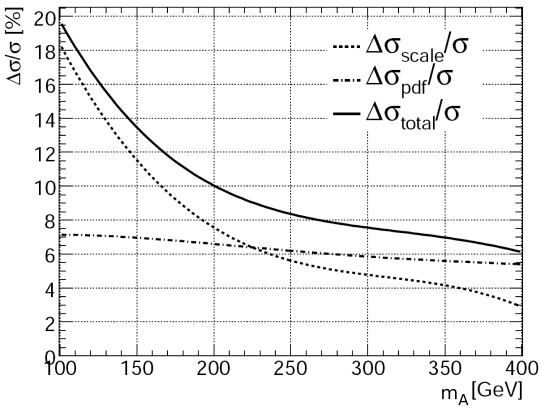

Figure 1: Systematic uncertainty on the signal cross-section for associated Higgs boson production as a function of m_A. The dashed line corresponds to the contribution from the scale uncertainty, the dash-dotted line to that introduced by the uncertainty on the parton distribution functions, and the solid line is the sum of both contributions added in quadrature.

2.2 Background processes

The following background processes are relevant and have been considered in this analysis (for details see Ref. [3]).

- $Z \to \ell\ell$: The Drell-Yan production of Z bosons and their subsequent decay into a pair of leptons constitutes an important source of background. The production cross-section has been calculated to NNLO accuracy and was found to be $\sigma_{Z\to\ell\ell} = (2015 \pm 60)$pb[2)] .

  Events with the Z boson decaying to a pair of τ leptons constitute an irreducible background. In particular for low Higgs boson masses, due to the limited invariant mass resolution in the $\tau^+\tau^-$ final state this background is problematic and needs therefore to be estimated directly from data.

[2)] The cross-section is given for a cut on the invariant mass of the lepton pair of $m_{\ell\ell} > 60$ GeV.

- $t\bar{t}$ production: The cross-section for this process has been calculated at NLO+NLL accuracy and was found to be $\sigma_{t\bar{t}} = (833 \pm 100)\,\text{pb}$. This background is dominant for Higgs boson masses beyond $m_A = 200$ GeV.

- W+jets production: The production cross-section for this process has been calculated at NNLO accuracy and was found to be $\sigma_{W+\text{Jets}} = 20510\,\text{pb}$. This dataset was complemented by a $Wb\bar{b}$ sample whose cross-section has been calculated to NLO accuracy ($\sigma_{Wb\bar{b}} = 176.9\,\text{pb}$).

2.3 Event generation

The Monte Carlo samples have been generated using the SHERPA [4], PYTHIA [5], HERWIG [6], ALPGEN [7], and MC@NLO [8] Monte Carlo generators. Except for SHERPA, all external matrix element generators are interfaced to HERWIG to produce the parton shower. The τ leptons are decayed using either SHERPA or TAUOLA [9]. Initial and final state radiation of photons is simulated using PHOTOS [10]. Event filters have been applied for all processes in order to increase the event generation efficiency. Details on Monte Carlo simulation are given in Ref. [3].

3 Analysis of the exclusive lepton lepton final state

The experimental signature consists of two leptons from the τ decays and missing transverse energy, $\not{E}_T$, due to the neutrinos from the τ decays. At least one jet tagged as coming from a b quark is required in the event and therefore the b quark associated production is dominant here.

3.1 Preselection

The preselection cuts are grouped into 'Trigger Selection', 'b-Tagging', 'Lepton Selection', and cuts related to the reconstruction of the invariant mass of the Higgs boson.

Trigger selection: An isolated muon (electron) with transverse momentum of at least 20 GeV (25 GeV) or two isolated electrons with $p_T \geq 15$ GeV, or one electron with $p_T \geq 15$ GeV and a muon with $p_T \geq 10$ GeV are required.

b-Tagging: Since the Higgs boson is produced in association with b quarks, at least one jet has to be identified as coming from a b quark in order to suppress backgrounds from processes involving light quarks. Jets are reconstructed using a cone algorithm with radius $\Delta R = 0.4$[3)], and a b-tagging weight of ≥ 3 is required in order for the jet to be labeled as coming from a b quark [11].

Lepton selection: Electrons are required to have $p_T \geq 10$ GeV, be within $|\eta| < 2.5$ and pass the medium electron selection [12]. No isolation criteria are applied. Muons are reconstructed using the algorithm described in Ref. [13]. A minimum p_T of 10 GeV and $|\eta| < 2.5$ are required. An isolation cone of opening angle $\Delta R = 0.2$ around the muon track is used with a maximum E_T of 6 GeV deposited in the calorimeters. Two leptons of opposite charge are required if the event is to be considered for further analysis. In case more than two leptons fulfill the above requirements the lepton pair with the highest scalar sum of p_T is selected.

[3)] The radius ΔR of the cone is defined as $\Delta R = \sqrt{\Delta\phi^2 + \Delta\eta^2}$

Collinear approximation: The invariant mass of the Higgs boson candidate is reconstructed using the collinear approximation [14]. In this approximation the masses of the particles involved in the decay of the τ lepton are small compared to their momenta, so that the direction of the τ lepton can be approximated by the direction of its observed visible decay products. The method assumes furthermore that the missing energy observed in the event is entirely due to neutrinos from the τ lepton decays. In addition the Higgs boson is required to have some amount of transverse momentum. If that is not the case the two τ leptons from the Higgs boson decay are back-to-back. An accurate reconstruction of the transverse momenta of the τ leptons is not possible in that case and the resolution of the invariant mass of the τ pair will be poor. Neglecting the masses of all leptons, the invariant mass of the Higgs boson candidate can be reconstructed via

$$m_{\tau^+\tau^-} = \frac{m_{\ell\ell}}{\sqrt{x_1 x_2}}. \quad (1)$$

The quantity $x_i = p_{T\,\ell_i}/p_{T\,\tau_i}$ is the fraction of the τ lepton momentum carried by its visible decay products. They are calculated from $\not\!\!E_T$ in the event and the transverse momentum of the visible leptons. For this calculation $\not\!\!E_T$ is decomposed into two components, each of them pointing along the direction of the charged decay products of the τ lepton. This fraction is required to be within physical bounds ($0 < x_i < 1$). In order for the solution to be numerically stable a cut on the angle between the visible decay products of the τ lepton of $\Delta\phi_{\ell\ell} < 3$ is imposed. This also improves the invariant $m_{\tau\tau}$ resolution.

The accepted cross-section for the above preselection is detailed in Table 2 for the signal and the dominant background contributions.

Table 2: Cross-section in fb passing the preselection criteria as described in the text. The numbers for the signal samples are given assuming $\tan\beta = 20$.

Process	Trigger	Lepton Selection	1 or 2 jets	>0 b-tags	Coll. Approx
$m_A = 110$ GeV	1837.6	1154.8	628.6	175.7	118.4
$m_A = 130$ GeV	1511.8	971.6	544.6	172.1	115.7
$m_A = 160$ GeV	987.4	656.4	374.9	119.1	80.8
$m_A = 200$ GeV	497.9	340	199.3	63.9	44.9
$m_A = 300$ GeV	139.4	98.8	60.2	20.4	13.9
$m_A = 450$ GeV	25.3	18.3	11.2	3.7	2.4
$t\bar{t}$	255114	48045.9	7804.8	5479	1096.2
$Z \to \tau\tau$	47026.8	27654.4	14053.2	665.1	440.6
$Z \to ee$	1.4 E6	797747	421393	16197.8	2848.4[4)]
$Z \to \mu\mu$	1.3 E6	704275	345491	16811.5	3223.4[4)]
W+Jets	17.2 E6	91042.8	44612.4	1537.5	122.4[4)]

3.2 Event selection

Cuts on kinematic variables have been optimized in an iterative procedure in order to maximize the statistical significance $S/\sqrt{B}$ for a potential Higgs boson signal. Since the composition of the background depends on the signal mass hypothesis, this has been done separately for each mass point. In addition, the optimization has been done separately for the ee, $\mu\mu$, and for the mixed $e\mu$ final states.

The following variables are considered: To suppress background from $t\bar{t}$ production only events with less than three jets are selected. The invariant dilepton mass $m_{\ell\ell}$ has to be well below m_Z in order to suppress $Z \to ee$ and $Z \to \mu\mu$ events. Since there are neutrinos from the τ decays in the event, missing transverse energy is required in the event. The transverse momentum of the jet tagged as coming from a b quark has to be above a certain value which depends on the Higgs boson mass under study.

[3)] Results were obtained using cut factorization.

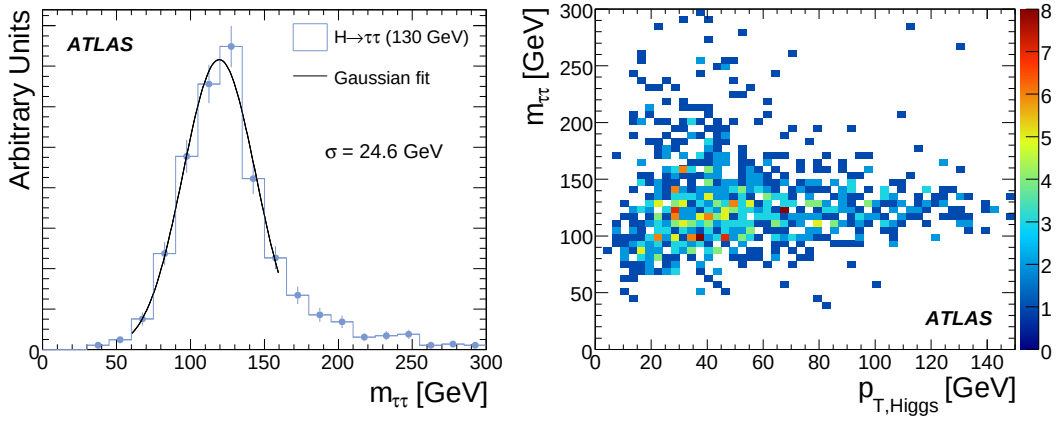

Figure 2: Invariant $m_{\tau^+\tau^-}$ distribution for a Higgs boson of mass $m_A = 130$ GeV (left) after preselection cuts. The width has been determined by a fit of a single Gaussian to the peak region of the distribution. The right-hand plot shows the $m_{\tau^+\tau^-}$ distribution as a function of the p_T of the Higgs boson.

Requirements on the maximum p_T of the leading lepton as well as on that of the lepton-lepton system $p_{T,\ell\ell}$ are imposed. In addition, the angle $\Delta\phi$ between the two leptons is restricted. The cut values and the accepted cross-section for a Higgs boson mass of $m_A = 130$ GeV are given in Table 3.

The resolution of the $m_{\tau^+\tau^-}$ distribution using the collinear approximation for a Higgs boson of mass $m_A = 130$ GeV is illustrated in Fig. 2 (left) after applying preselection cuts. The width as extracted from a fit of a single Gaussian to the peak region is $\sigma = 25$ GeV compared to the natural width of a Higgs boson of that mass between less than 100 MeV up to a few GeV depending on $\tan\beta$. The $m_{\tau^+\tau^-}$ distribution versus the p_T of the Higgs boson is illustrated on the right-hand side of Fig. 2, showing that the invariant mass resolution improves with p_T of the Higgs boson.

3.3 Selection results

The accepted cross-sections after all cuts for different Higgs boson masses and the various backgrounds are summarized in Table 4 for $\tan\beta = 20$. The reconstructed $\tau\tau$ invariant mass distributions are displayed in Fig. 3 for all masses considered. The vertical solid lines mark the mass window defined as $m - 1.65\sigma < m_{\tau^+\tau^-} < m + 2\sigma$ where σ denotes the invariant $m_{\tau^+\tau^-}$ resolution for a given mass hypothesis as determined from Monte Carlo simulations. All candidate events falling inside this mass window are used to calculate the significances for a Higgs boson signal.

In the low mass range, the invariant mass resolution is of the order of 25 GeV. A potential signal for a Higgs boson is nearly indistinguishable from the irreducible $Z \to \tau^+\tau^-$ background which dominates in this mass range over the contribution from $t\bar{t}$ processes, which contribute at the $(10-20)\%$ level. This makes it necessary to estimate the shape and the normalization of the $Z \to \tau^+\tau^-$ background directly from data. A procedure has been developed and will be discussed in detail in Section 3.5.

In the medium mass range, the contributions from $Z \to \tau^+\tau^-$ events and from $t\bar{t}$ processes become equally important. The mass resolution for signal events is now of the order of $(30-40)$ GeV leading to a broad structure which is indistinguishable from that of background events.

In the high mass range ($m_A = 300$ to 450 GeV), the cross-section for the signal process decreases rapidly. The invariant mass resolution for signal events is between $(50-80)$ GeV so that a discovery with an integrated luminosity of $\mathscr{L} = 30\,\text{fb}^{-1}$ in this channel will not be possible.

Table 3: Accepted cross-section in fb for optimized cuts for $m_A = 130$ GeV and $\tan\beta = 20$. The values of the cuts applied are stated for the $ee/\mu\mu$ (upper row) and $e\mu$ (lower row) subchannels. In case only one number is given it applies to all leptonic subchannels.

Variable	Selection	$H \to \tau\tau$	$t\bar{t}$	$Z \to \tau\tau$	$Z \to ee$	$Z \to \mu\mu$	W+Jets
Precuts		115.7±5.1	1096±35	441±16	3223±123	2848±108	122±40
p_T b-jet	$(15-66)$ GeV	90.0±4.5	443±22	337±14	2756±113	2481±101	91±35
$m_{\ell\ell}$	$(27-70)$ GeV $(0-70)$ GeV	72.6±4.1	138±12	326±14	134±25	92±19	60±28
$x_1 \cdot x_2$	$(0.04-0.4)$ $(0.0-0.5)$	64.1±3.8	108±11	251±12	47±15	36±12	40±23
$p_{\mathrm{T}}^{\mathrm{miss}}$	$(20-\infty)$ GeV $(15-\infty)$ GeV	52.2±3.5	102±11	171±10	4.3±4.5	5.1±4.6	33±21
p_{T}^{H}	$(0-\infty)$ GeV $(0-70)$ GeV	47.7±3.3	57.9±7.9	159.4±9.8	4.3±4.5	4.6±4.3	28±19
$p_{\mathrm{T},\ell\ell}$	$(0-45)$ GeV $(0-60)$ GeV	46.5±3.3	38.2±6.5	155.8±9.6	3.9±4.3	2.5±3.2	23±17
$\Delta\Phi_{\ell\ell}$	$(2.24-3)$ $(2-3)$	43.3±3.1	32.8±6.0	107.5±8.0	3.6±4.1	3.8±4.0	21±17
p_T leading ℓ	$(10-80)$ GeV	43.3±3.1	32.8±6.0	107.5±8.0	3.6±4.1	3.8±4.0	21±17
Mass Window	$(111-198)$ GeV	28.4±2.6	19.7±4.6	22.1±3.6	1.8±2.9	2.0±2.8	12±12

Table 4: Accepted cross-section for all Higgs boson mass hypotheses analyzed. The cross-section in fb for signal and background after all selection cuts is given (except for the cut on the mass window) for $\tan\beta = 20$.

	$H \to \tau^+\tau^-$	$t\bar{t}$	$Z \to \tau^+\tau^-$	$Z \to e+e^-$	$Z \to \mu^+\mu^-$	W+jets
$m_A = 110$ GeV	34.4 ± 2.9	24.0 ± 5.1	62.1 ± 6.1	1.9 ± 3.0	2.7 ± 3.3	8 ± 11
$m_A = 130$ GeV	28.4 ± 2.6	19.7 ± 4.6	22.1 ± 3.6	1.8 ± 2.9	2.0 ± 2.8	12 ± 12
$m_A = 160$ GeV	18.7 ± 1.2	39.3 ± 6.6	8.4 ± 2.2	1.4 ± 2.5	2.0 ± 2.9	1.8 ± 4.9
$m_A = 200$ GeV	10.9 ± 0.6	28.4 ± 5.6	5.4 ± 1.8	2.0 ± 3.1	2.1 ± 2.9	3.7 ± 7.0
$m_A = 300$ GeV	2.7 ± 0.1	32.8 ± 6.0	3.0 ± 1.3	0.4 ± 1.4	1.7 ± 2.6	5.8 ± 8.8
$m_A = 450$ GeV	0.50 ± 0.03	50.2 ± 7.4	1.8 ± 1.0	0.4 ± 1.4	0.3 ± 1.1	4.1 ± 7.3

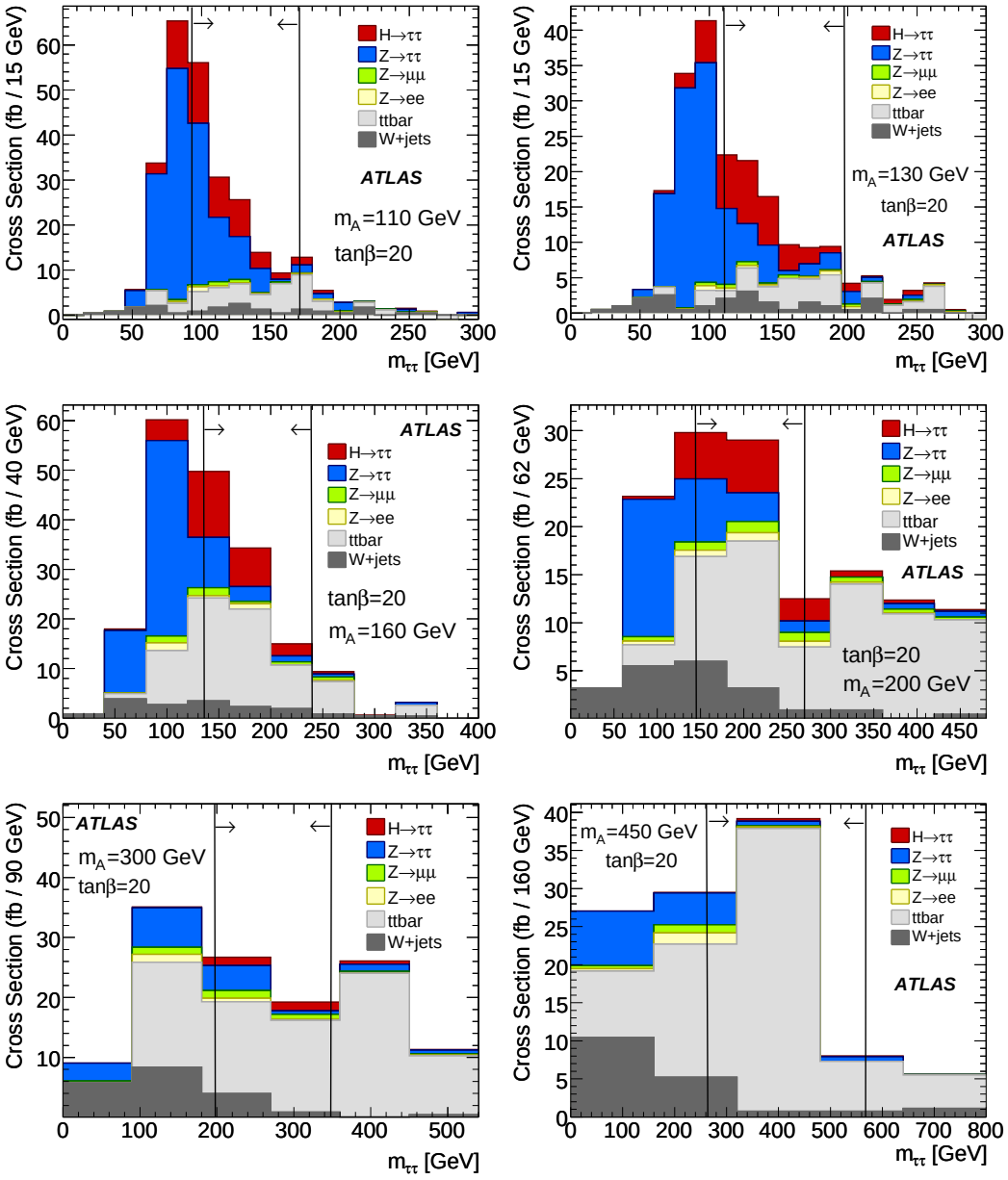

Figure 3: Invariant $m_{\tau^+\tau^-}$ distribution for signal and background events. The distributions are shown after all selection cuts with the nominal masses and $\tan\beta$ values as indicated in the plots. The vertical lines indicate the mass window used for calculating the signal significance.

3.4 Systematic uncertainties

Table 5: Effects of systematic uncertainties as described in the text for different Higgs boson masses for $\tan\beta = 20$. The effects of the systematic uncertainties considered are listed in percent. The total uncertainty is obtained by adding the individual contributions in quadrature.

	$m_A = 110$ GeV			$m_A = 130$ GeV			$m_A = 160$ GeV		
Uncertainty / %	Signal	$t\bar{t}$ Bkg	W+jets	Signal	$t\bar{t}$ Bkg	W+jets	Signal	$t\bar{t}$ Bkg	W+jets
b-tagging efficiency	2.8	3.9	0.8	4.0	4.1	0.7	6.6	3.3	0.5
Jet energy scale	0.3	6.0	0.9	< 0.1	5.3	1.6	1.1	4.0	1.5
Jet resolution	8.3	0.8	0.3	< 0.1	0.2	1.2	6.1	0.4	1.2
Electron energy scale	0.7	0.5	1.0	0.4	0.1	1.0	0.4	0.5	0.9
Electron resolution	0.7	0.6	1.0	1.6	0.2	1.0	0.4	0.2	0.4
Muon energy scale	0.7	0.9	0.7	1.2	0.6	0.7	0.4	0.4	0.7
Muon resolution	1.4	0.6	2.5	0.8	1.1	2.4	1.7	0.4	2.4
Electron efficiency	< 0.1	0.5	0.4	< 0.1	0.5	0.4	< 0.1	0.4	0.4
Muon efficiency	< 0.1	0.8	0.7	0.8	0.2	0.7	< 0.1	0.9	0.7
Light jet rejection	< 0.1	< 0.1	3.4	0.4	< 0.1	3.4	0.7	< 0.1	3.4
Total exp. uncertainty	9	7.4	4.7	4.6	6.8	4.9	9.2	5.3	4.8

	$m_A = 200$ GeV			$m_A = 300$ GeV			$m_A = 450$ GeV		
Uncertainty / %	Signal	$t\bar{t}$ Bkg	W+jets	Signal	$t\bar{t}$ Bkg	W+jets	Signal	$t\bar{t}$ Bkg	W+jets
b-tagging efficiency	4.8	3.2	0.5	4.2	3.1	0.3	4.8	3.8	0.1
Jet energy scale	0.6	3.6	1.5	0.9	3.1	0.6	0.4	2.1	0.7
Jet resolution	8.0	1.6	2.7	0.8	0.4	2.7	0.7	0.5	2.4
Electron energy scale	0.5	0.5	0.9	< 0.1	0.2	0.8	0.4	0.2	1.2
Electron resolution	0.3	0.1	0.4	< 0.1	< 0.1	0.3	< 0.1	0.4	0.3
Muon energy scale	0.5	0.4	0.7	0.5	0.4	0.7	0.9	0.3	0.9
Muon resolution	0.3	0.1	2.4	0.8	0.3	2.3	0.4	0.7	2.2
Electron efficiency	0.3	0.3	0.4	0.8	< 0.1	0.4	0.4	0.1	0.4
Muon efficiency	0.3	1.0	0.7	0.8	1.3	0.7	1.1	1.0	0.7
Light jet rejection	0.8	< 0.1	3.4	0.4	< 0.1	3.4	0.4	< 0.1	3.4
Total exp. uncertainty	9.4	5.3	5.4	4.6	4.7	5.1	5.1	4.6	5.1

In order to assess the impact of systematic uncertainties, each of these has been applied in turn and the impact on the result of the analysis is evaluated. The uncertainties assumed on the energy and momentum resolution of muons, electrons, photons, and jets are conservative estimates assuming non-optimal performance of the corresponding algorithms at the beginning of data taking.

1. For muons the uncertainty on the reconstructed p_T is $\sigma(1/p_T) = (0.011/p_T \otimes 0.00017)$ with p_T given in GeV. The uncertainty on the energy scale is estimated to be $\pm 1\%$, and that on the reconstruction efficiency is assumed to be 1% and flat in p_T.

2. For electrons and photons the uncertainty on the reconstructed E_T is $\sigma(E_T) = 0.0073 \cdot E_T$. The uncertainty on the energy scale is estimated to be $\pm 0.5\%$, and that on the reconstruction efficiency is assumed to be 0.2% and being flat in E_T.

3. For jets with $|\eta| < 3.2$ ($|\eta| > 3.2$) the uncertainty on the jet energy scale is taken to be $\pm 3\%$ ($\pm 10\%$) and the jet energy resolution is assumed to be $45\%\sqrt{E}$ ($63\%\sqrt{E}$).

4. For the b-tagging a degradation of the tagging efficiencies of 5% is taken as systematic uncertainty. For the Z+light jets background an uncertainty on the rejection rate of $\pm 10\%$ is assumed.

A detailed description of the sources of systematic uncertainties can be found in [3]. The impact of the systematic uncertainties on the number of signal and $t\bar{t}$ background events[5)] inside the mass window is summarized in Table 5 for Higgs boson masses between $m_A = 110$ and 450 GeV. A sample of 48 M $t\bar{t}$ events from fast simulation has been used for these studies. The $Z \to \tau\tau$ background in this analysis is estimated from sidebands in data as described in the next Section. The number of events from $Z \to \mu\mu$ and $Z \to ee$ processes after all selection cuts is small compared to that from $t\bar{t}$. Their contribution to the total systematic uncertainty is small compared to that from $t\bar{t}$ processes.

3.5 Estimation of $Z \to \tau^+\tau^-$ shape and normalization from data

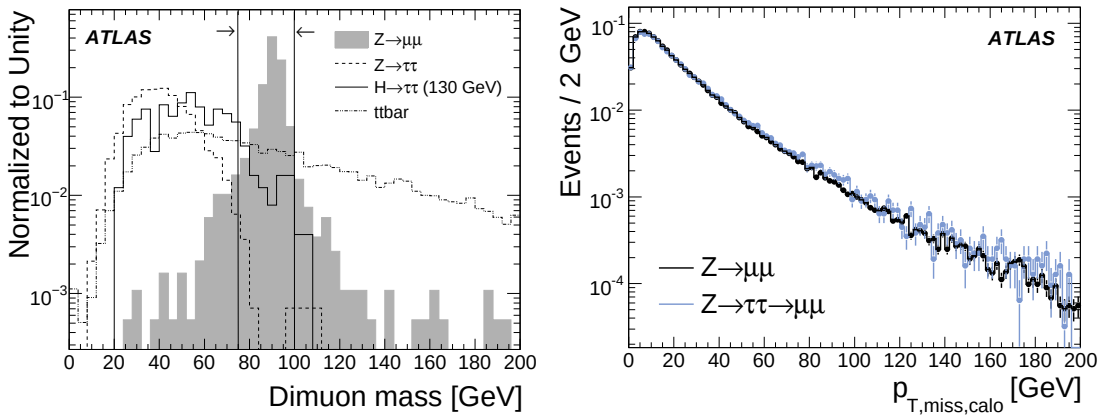

Figure 4: Distribution of the invariant dilepton mass $m_{\ell\ell}$ (left). The shaded area illustrates the distribution from $Z \to \mu\mu$ events, and the solid line that from signal events. The contribution from $Z \to \tau^+\tau^-$ and $t\bar{t}$ events is illustrated by the dashed and dotted lines, respectively. The cut on the invariant $\ell\ell$ mass is indicated by the solid vertical lines. The distribution of p_T^{miss} in the calorimeter for $Z \to \mu\mu$ and $Z \to \tau\tau \to \mu\mu + X$ events (right). All plots shown are after preselection cuts.

As discussed above the estimation of the shape and the normalization of the irreducible $Z \to \tau^+\tau^-$ events from data is of great importance in particular for low Higgs boson masses where this background is dominant. Procedures to estimate both the shape and the normalization of $Z \to \tau^+\tau^-$ events from data are needed. This procedure is based on $Z \to \mu\mu$ and $Z \to ee$ events selected from a sideband region which is free of Higgs boson events, in contrast to the signal region. The method proceeds in three steps:

1. As a first step, a pure sample of $Z \to \mu\mu$ or $Z \to ee$ events is selected from a sideband region as described below.

2. The shape of the $m_{\tau\tau}$ spectrum is estimated by adapting the four-momenta of the muons such that they appear like coming from $Z \to \tau\tau$ events.

3. The normalization of the $Z \to \tau\tau$ background is estimated from a double-ratio comparing the number events found in data and in Monte Carlo in the sideband region as well as in the signal region.

This procedure is described in detail below.

[5)] The impact on the number of $Z \to \tau^+\tau^-$ events is not listed here since this background is estimated from data.

3.5.1 Definition of signal and sideband regions

Events of the type $Z \to ee$ and $Z \to \mu\mu$ are selected from a sideband region (called region B) with very high purity and with an event topology similar to that from $Z \to \tau^+\tau^-$ events in the signal region (called region A). The following cuts are applied in order to select $Z \to ee$ and $Z \to \mu\mu$ events in region B:

- The invariant mass of the lepton-lepton system is required to be within 75 GeV $< m_{\ell\ell} <$ 100 GeV, where $\ell\ell$ is either a ee or a $\mu\mu$ final state.
- At least one jet identified as coming from a b quark has to be found in the event.
- The number of jets allowed in the event has to be less than three.

The main cut defining region B is that on the invariant lepton-lepton mass. A distribution illustrating the cut on $m_{\ell\ell}$ is displayed in Fig. 4 (left) showing the large amount of $Z \to \mu\mu$ events selected by the cuts above that only have a small contamination of events coming from $t\bar{t}$ processes and events containing Higgs boson decays. The number of events from $Z \to ee$ and $Z \to \mu\mu$ is around 500 000 for an integrated luminosity of 30 fb^{-1} and thus much larger than the number of $Z \to \tau\tau$ events expected in the signal region. The purity of the $Z \to \mu\mu$ ($Z \to ee$) control sample in region B after all cuts mentioned above is 99.1% (97.9%) with a contribution of 0.04% (0.05%) of events from the signal process[6)] with the remainder coming from $t\bar{t}$ processes.

3.5.2 Estimation of the $Z \to \tau^+\tau^-$ shape from data

The method of estimating the shape of $Z \to \tau^+\tau^-$ events from data is based on the assumption that in the calorimeter this type of events is indistinguishable from that of type $Z \to \mu\mu$. This method has been proven to work in a vector boson fusion $H \to \tau^+\tau^-$ analysis [15].

The muons are minimum ionizing particles and their energy deposit in the calorimeter only weakly depends on their momentum. Therefore, the missing energy signatures of both types of events in this detector component are very similar as illustrated on the right-hand side of Fig. 4. Altering the energy of muons in $Z \to \mu\mu$ events so that they correspond to those from $Z \to \tau^+\tau^- \to \mu\mu + 4\nu$ events leads to identical distributions of $p_{T,\mu}$, $p_{T,\mathrm{miss}}$ and $m_{\tau^+\tau^-}$ for both classes of events. The following procedure is adopted:

- Three dimensional reference histograms from $Z \to \tau^+\tau^- \to \mu\mu + 4\nu$ events from Monte Carlo in region A are created. The following variables calculated in the Z rest frame are used:
  1. The absolute value of the Gottfried-Jackson angle ξ between the Z boson and the negatively charged muon.
  2. The energy of the muon with $\cos\xi > 0$.
  3. The energy of the muon with $\cos\xi < 0$.
- The components of the momentum vector of the muons in $Z \to \mu\mu$ events from region B are altered in a way that they match those from $Z \to \tau^+\tau^- \to \mu\mu + 4\nu$ events using the above reference histogram:

$$p_{i,\mathrm{altered}} = \frac{p_i}{|\vec{p}|} \cdot E_{\mu,\mathrm{altered}}. \tag{2}$$

  For each event, the angle ξ is calculated and then new energies for the muons are chosen randomly from the reference histogram. After applying this procedure, the muon momenta are boosted back into the lab frame.

[6)] A Higgs boson mass of $m_A = 130$ GeV and $\tan\beta = 20$ is assumed here. The contamination of Higgs boson events is even smaller for the other signal masses considered in this analysis.

- The missing energy in the event is re-calculated according to the new muon momenta:

$$\vec{p}_{T,\mathrm{miss,altered}} = \vec{p}_{T,\mathrm{miss}} - \sum_{\mu} p_{T,\mathrm{altered}} + \sum_{\mu} p_{T,\mathrm{old}}. \tag{3}$$

A comparison of $p_{\mathrm{T,miss}}$, of $x_1 \cdot x_2$ from the collinear approximation and of the invariant $m_{\tau^+\tau^-}$ mass from altered $Z \to \mu\mu$ in comparison with $Z \to \tau^+\tau^- \to \mu\mu + 4\nu$ events is shown on the left-hand side, middle and right-hand side of Fig. 5, respectively. Good agreement within the statistical uncertainties of the samples used is observed.

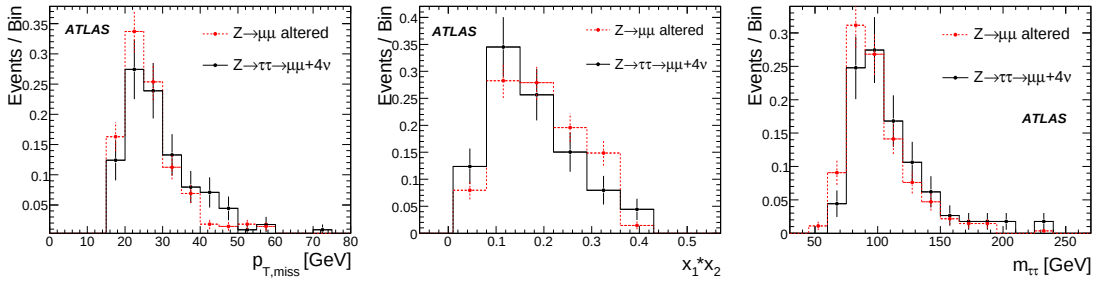

Figure 5: Comparison of the $p_{\mathrm{T,miss}}$, $x_1 \cdot x_1$, and $m_{\tau\tau}$ spectra for events of type $Z \to \mu\mu$ and $Z \to \tau\tau$. Good agreement within the statistical uncertainties is observed.

The same shape as extracted from region B using $Z \to \mu\mu$ events to estimate $Z \to \tau\tau \to \mu\mu + X$ events in region A is also used for $Z \to \tau\tau \to ee + X$ and $Z \to \tau\tau \to \mu e + X$ events. As shown in Figure 6, the $m_{\tau\tau}$ shapes are identical within statistical uncertainties justifying this procedure.

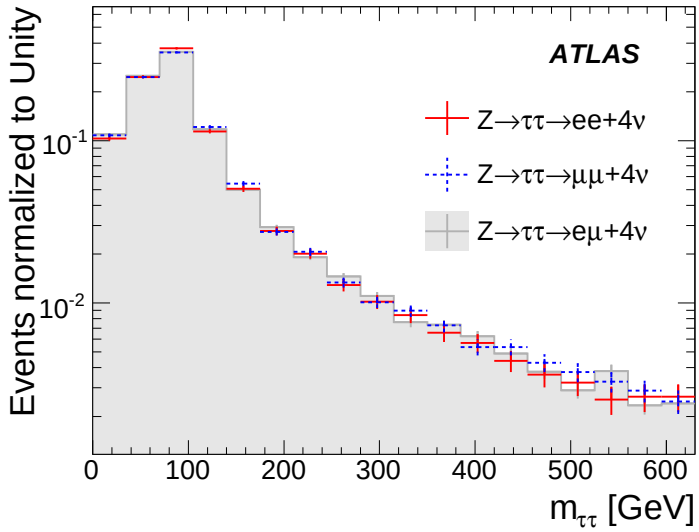

Figure 6: Comparison of the $m_{\tau\tau}$ shape for $Z \to \tau\tau \to \mu\mu + X$, $Z \to \tau\tau \to ee + X$, and $Z \to \tau\tau \to \mu e + X$ events. Good agreement is observed within the statistical uncertainties of the samples used.

3.5.3 Estimation of the background normalization from data

In order to estimate the number of background events from the $Z \to \tau^+\tau^-$ background process for this analysis, the same definition of the sideband region has been used as described above.

The number of $Z \to \tau^+\tau^-$ background events in the signal region A can then be obtained by re-weighting the number of events found in data in region B by the predicted ratio of the number of events found in Monte Carlo in region A relative to that found in region B. In order for this method to be valid, the following two conditions have to hold:

$$\frac{(Z \to \ell\ell)^{\mathrm{B}}_{\mathrm{Data}}}{(Z \to \ell\ell)^{\mathrm{B}}_{\mathrm{MC}}} = \frac{(Z \to \tau^+\tau^- \to \ell\ell + 4\nu)^{\mathrm{B}}_{\mathrm{Data}}}{(Z \to \tau^+\tau^- \to \ell\ell + 4\nu)^{\mathrm{B}}_{\mathrm{MC}}} \tag{4}$$

$$\frac{(Z \to \ell\ell)^{\mathrm{B}}_{\mathrm{Data}}}{(Z \to \ell\ell)^{\mathrm{B}}_{\mathrm{MC}}} = \frac{(Z \to \tau^+\tau^- \to \ell\ell + 4\nu)^{\mathrm{A}}_{\mathrm{Data}}}{(Z \to \tau^+\tau^- \to \ell\ell + 4\nu)^{\mathrm{A}}_{\mathrm{MC}}}, \tag{5}$$

where the first condition means that $Z \to \ell\ell$ events behave like $Z \to \tau^+\tau^- \to \ell\ell + 4\nu$ events, and when combined with the second it implies that $Z \to \tau^+\tau^- \to \ell\ell + 4\nu$ events in region A and in region B behave identically.

The calculation of the number of events from the $Z \to \tau^+\tau^-$ process in data is performed in bins of p_T of the leading lepton vs. the p_T of the subleading lepton with a bin size of $2 \times 2\ \mathrm{GeV}^2$ which was found to give unbiased results in previous Monte Carlo based studies [16]. This ensures that the method is less dependent on the differences in p_T in the signal and the sideband region. Once events from real data are available the method has to be validated and the influence of a possible difference between data and the Monte Carlo prediction on the results has to be checked.

This procedure also allows to easily take into account differences in acceptance and trigger efficiencies by simply applying the appropriate factors to the reweighting procedure. The number of $Z \to \tau^+\tau^- \to \ell\ell + 4\nu$ events in region A is then given by

$$(Z \to \tau^+\tau^- \to \ell\ell + 4\nu)^{\mathrm{A}}_{\mathrm{Data}} = \sum_{i,j} \frac{\left((Z \to \tau^+\tau^- \to \ell\ell + 4\nu)^{\mathrm{A}}_{\mathrm{MC}}\right)_{ij}}{\left((Z \to \ell\ell)^{\mathrm{B}}_{\mathrm{MC}}\right)_{ij}} \cdot \left((Z \to \ell\ell)^{\mathrm{B}}_{\mathrm{Data}}\right)_{ij}, \tag{6}$$

where i and j indicate the corresponding bin in p_T. The statistical uncertainty on this method is calculated according to Gaussian error propagation. The method has been tested using two independent Monte Carlo samples, one to fill the reference histogram and one to test the reweighting procedure. Good agreement within statistical uncertainties between the expected number of events in region A and that actually found was observed.

The application of this method is straight forward for the ee and the $\mu\mu$ final state. For the $e\mu$ final state the procedure has to be adapted since there are no $Z \to e\mu$ decays. In order to estimate the number of background events in that case, events from $Z \to ee$ and $Z \to \mu\mu$ processes are used. Additional correction factors are applied to account for the differences in trigger efficiencies and selection efficiencies in that case.

3.5.4 Systematic uncertainties of the background estimation procedure

The impact of the systematic uncertainties on the estimation of the number of background events from $Z \to \tau^+\tau^-$ processes as described in Section 3.4 has been evaluated. The uncertainties on jet energy scale and jet resolution, as well as on the b tagging efficiency are expected to be negligible since the same effects would apply to the signal region as well as to the sideband region. The remaining contributions to the systematic uncertainty on the background estimation procedure are coming from the energy scale, efficiency and resolution connected with the electrons and muons in the final state. These contributions as expected in $30\,\mathrm{fb}^{-1}$ of data are summarized in Table 6.

In addition, systematic uncertainties due to the different acceptances and trigger efficiencies for the $Z \to ee/\mu\mu$ samples from the sideband region compared to $Z \to \tau\tau \to ee/\mu\mu/e\mu + X$ samples in the signal region need to be taken into account. Since the reweighting of events is done as a function of the

Table 6: The effects of systematic uncertainties on the calculation of the normalization.

Uncertainty Effect	Value	Systematic Uncertainty
Muon resolution	$\sigma\left(\frac{1}{p_T}\right) = \sqrt{\left(\frac{0.011}{p_T}\right)^2 + 0.00017^2}$	0.16 %
Muon energy scale	$\pm 1\%$	1.35 %
Muon efficiency	$\pm 1\%$	0.7 %
Electron resolution	$\sigma(E_T) = 0.0073 \cdot E_T$	1.9 %
Electron energy scale	$\pm 0.5\%$	0.85 %
Electron efficiency	$\pm 0.2\%$	0.1 %

p_T of the leading and the subleading lepton, these are easy to apply. Since this analysis is aimed at an integrated luminosity of $30\,\text{fb}^{-1}$, it is assumed that by then these uncertainties are evaluated to a very high precision.

The overall systematic uncertainty has been evaluated to be 2.6% by dividing the available MC events into two independent samples. This uncertainty has been taken into account for the final results.

3.5.5 Summary of the background estimate from data

Both methods described above are now combined to estimate the $Z \to \tau\tau$ background and thereby the significance of a possible Higgs boson signal in the low mass region. First, the number of events of type $Z \to \tau^+\tau^-$ is estimated using the method described in Section 3.5.3. Then, the shape of this background is determined as described in Section 3.5.2. The background is then subtracted from the $m_{\tau^+\tau^-}$ distribution.

3.6 Results and discovery potential

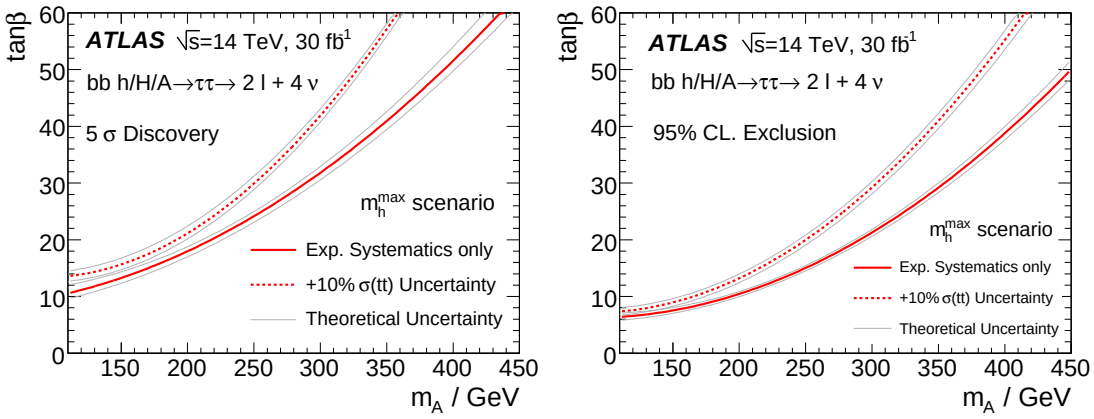

Figure 7: The five σ discovery potential (left) and the 95% exclusion limit (right) as a function of m_A and $\tan\beta$. The solid line represents the main result of the analysis. The dashed lines indicate the discovery potential and exclusion limit including an addition 10% uncertainty on the $t\bar{t}$ cross-section. The bands represent the influence of the systematic uncertainty on the signal cross-section.

The discovery potential for the $h/H/A \to \tau^+\tau^- \to \ell\ell 4\nu$ channel is now assessed. All sub-channels, i.e. ee, $e\mu$ and $\mu\mu$ are combined to calculate the significance of a Higgs boson signal. A mass window

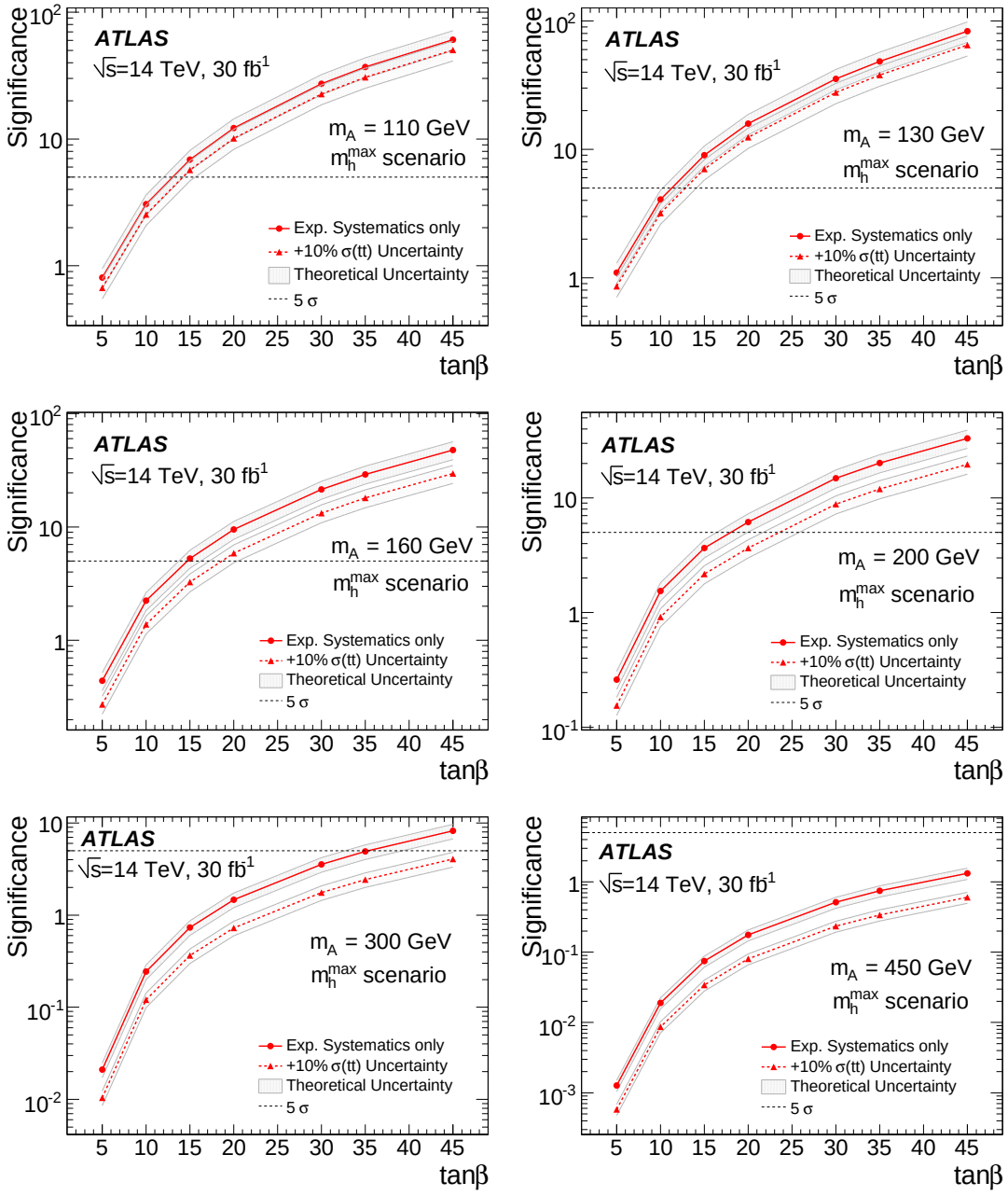

Figure 8: The discovery potential as a function of $\tan\beta$ and for Higgs boson masses as indicated in the plots. The solid lines indicate the discovery potential including experimental systematic uncertainties. The dashed lines indicate the discovery potential including an additional systematic uncertainty on the $t\bar{t}$ cross-section. The bands indicate the impact of the systematic uncertainty on the signal cross-section.

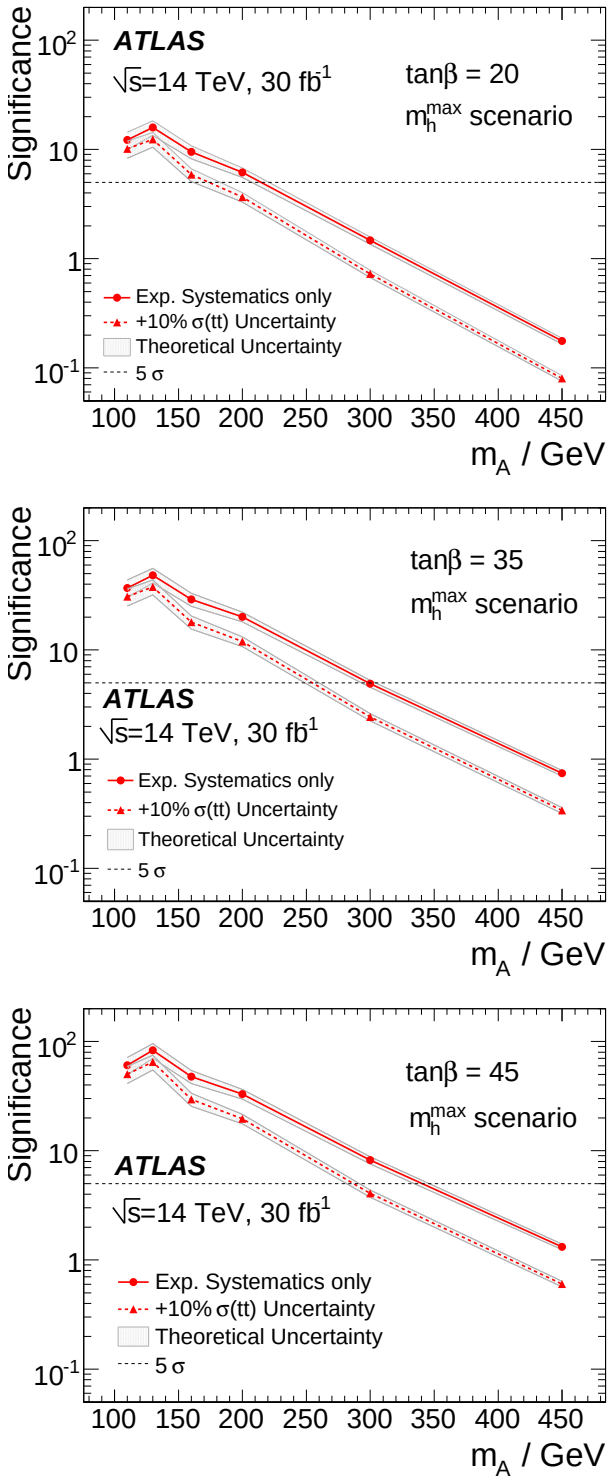

Figure 9: The discovery potential as a function of m_A. The solid lines indicate the discovery potential including experimental systematic uncertainties for $\tan\beta$ values as indicated in the plots. The dashed lines indicate the discovery potential including an additional systematic uncertainty on the $t\bar{t}$ cross-section of 10%. The bands indicate the impact of the systematic uncertainty on the signal cross-section.

$m - 1.65\sigma < m_{\tau^+\tau^-} < m + 2\sigma$ is applied to calculate the final significance where σ denotes the invariant mass resolution of the Higgs boson signal of the corresponding mass.

The shape and the normalization of the $Z \to \tau^+\tau^-$ background is estimated from the sideband region in data as described in Section 3.5. There is no corresponding procedure available yet for the $t\bar{t}$ background so that all experimental systematic uncertainties are taken into account for all calculations below. Theoretical uncertainties are treated separately. The significance of a potential Higgs boson signal in the given mass window is calculated as

$$\text{Sign.} = \frac{S}{\sqrt{N_{t\bar{t}} + (\Delta_{\text{sys}}^{t\bar{t}})^2 + N_{\text{Z}\to\tau\tau} + (\Delta_{\text{sys}}^{Z\to\tau\tau})^2 + N_{\text{W}\to\ell\nu} + (\Delta_{\text{sys}}^{W\to\ell\nu})^2 + N_{\text{Z}\to\text{ee}} + N_{\text{Z}\to\mu\mu}}}, \qquad (7)$$

where S is the number of signal events, $N_{t\bar{t}}$ and $\Delta_{\text{sys}}(t\bar{t})$ are the statistical and systematic uncertainties on the $t\bar{t}$ background. The quantities $N_{Z\to\tau^+\tau^-}$ and $\Delta_{\text{sys}}(Z \to \tau^+\tau^-)$ are the statistical and systematic uncertainties on the $Z \to \tau^+\tau^-$ background, respectively. The term in the denominator is dominated by the contribution from $t\bar{t}$ events; the contributions from $N_{\text{Z}\to\text{ee}}$ and $N_{\text{Z}\to\mu\mu}$ and their corresponding systematic uncertainties are negligible.

The discovery potential and the 95% exclusion limit in the m_h^{max} scenario as a function of $\tan\beta$ and m_A and for an integrated luminosity of $30\,\text{fb}^{-1}$ is displayed in Fig. 7 on the left-hand side and right-hand side, respectively. The uncertainty on the signal cross-section is indicated as bands in the plots. The calculation of the significance includes both statistical and experimental systematic uncertainties on the background. The uncertainties on the background cross-sections are not taken into account in the main results since they are assumed to be measured with high precision at the time of the analysis. However, since the cross-section for the $t\bar{t}$ background might not be measured at high precision in the region of phase space relevant to this analysis, the discovery potential including a 10% uncertainty on that background is displayed in addition (dashed line).

The discovery potential for Higgs bosons is shown in Fig. 8 as a function of $\tan\beta$ for various m_A values, and in Fig. 9 as a function of m_A for various $\tan\beta$ values.

4 Conclusion

In this note a study of the discovery potential for the supersymmetric Higgs bosons $h/H/A$ in proton-proton collisions at a center-of-mass energy of 14 TeV with the ATLAS detector at the LHC has been presented. The final state $h/H/A \to \tau^+\tau^-$ in b quark associated production has been investigated with at least one jet identified as coming from a b quark and with both τ leptons decaying leptonically.

A significant improvement for the discovery potential can be achieved if this channel is combined with the ℓ-had and had-had channel, where one τ lepton decays leptonically (either electron or muon) and one hadronically, or both τ leptons decay hadronically [17].

References

[1] Carena, M. S. and Heinemeyer, S. and Wagner, C. E. M. and Weiglein, G., Eur. Phys. J. **C26** (2003) 601–607.

[2] Harlander, R. V. and Kilgore, W. B., Phys. Rev. D **68** (2003) 013001.

[3] ATLAS Collaboration, *Cross-Sections, Monte Carlo Simulations and Systematic Uncertainties*, this volume.

[4] Gleisberg, Tanju et al., JHEP **02** (2004) 056.

[5] Sjostrand, T. et al., Comput. Phys. Commun. **135** (2001) 238–259.

[6] Marchesini, G. and Webber, B. R., Cavendish-HEP-87/9 (1987).

[7] Mangano, M. L. and Moretti, M., and Piccinini, F. and Pittau, R. and Polosa, A. D., JHEP **07** (2003) 001.

[8] Frixione, S. and Webber, B. R., hep-ph/0207182 (2002).

[9] Jadach, S. and Kuhn, J. H. and Was, Z., Comput. Phys. Commun. **64** (1990) 275–299.

[10] Barberio, E. and van Eijk, B. and Was, Z., Comput. Phys. Commun. **66** (1991) 115–128.

[11] ATLAS Collaboration, *b-Tagging Performance*, this volume.

[12] ATLAS Collaboration, *Reconstruction and Identification of Electrons*, this volume.

[13] ATLAS Collaboration, *Muon Reconstruction and Identification: Studies with Simulated Monte Carlo Samples*, this volume.

[14] Ellis, R. K. and Hinchliffe, I. and Soldate, M. and van der Bij, J. J., Nucl. Phys. **B297** (1988) 221.

[15] M. Schmitz, *Studie zur Bestimmung des Untergrundes aus Daten und der Higgs-Boson-Masse in Vektorbosonfusion mit $H \to \tau\tau \to \mu\mu + 4\nu$ mit dem ATLAS-Detektor*, Internal Report BONN-IB-2006-07 (2006), Bonn University, 2006.

[16] J. Schaarschmidt, *A Study of b Quark Associated Higgs Production in the Decay Mode $h/H/A \to \tau\tau \to 2\ell + 4\nu$ with ATLAS at LHC*, Internal report, Technische Universität Dresden, 2007.

[17] ATLAS: Detector and physics performance technical design report. Volume 2, CERN-LHCC-99-15.